Reversible restructuring of supported Au nanoparticles during butadiene hydrogenation revealed by *operando* GISAXS/GIWAXS

David James Martin[1,2], Yaroslav I. Odarchenko[1,2], Donato Decarolis[1,2], Jennifer J. Herbert[1,2,3], Thomas Arnold[4], Jonathan Rawle[4], Chris Nicklin[4], Hans-Gerd Boyen[5] and Andrew M. Beale[1,2*]

[1] Department of Chemistry, University College London, 20 Gordon Street, London, WC1H 0AJ, UK
[2] Research Complex at Harwell (RCaH), Harwell, Didcot, Oxfordshire OX11 0FA, UK
[3] Netherlands Organisation for Scientific Research (NWO), DUBBLE CRG@ESRF, Grenoble 38042, France
[4] Diamond Light Source, Harwell Science and Innovation Campus, Chilton, Didcot OX11 0DE, UK
[5] Institute for Materials Research, Hasselt University, Diepenbeek, Belgium

*Correspondence to be directed to Andrew.Beale@ucl.ac.uk

Experimental methodology

Sample preparation

Nanoparticles synthesis: Au nanoparticles with regular periodicity (δ) and particle size of 9.0 ± 0.9 nm were prepared using the reverse micelle method[1]. Briefly, PS-b-P2VP (Polymer Source Inc.) was dispersed in toluene (Riedel de Haën, 99.5%) at a concentration of 5 mg/ml, and stirred for one week to achieve complete dissolution. Subsequently, chloroauric acid (HAuCl4 • H2O, Sigma-Aldrich, 99.999%) was added to the micelle-toluene solution. The metal loading took place in a nitrogen-filled glovebox with relative humidity below 10% to avoid phase separation. This final solution was stirred for another week and then filtered through a 1 µm (Glass Fibre GF100/25) and 2 µm filter (PTFE O-20/25), both from Macherey Nagel, to remove any polymer aggregates.

Catalyst preparation: Model catalysts were prepared by depositing AuNPs on the flat single crystal Si(111) substrate. Silicon wafers (1 cm², n-type) were cleaned and subsequently dip coated at a withdrawal rate of 10 mm/min. The dried silicon substrates were then plasma etched using a custom built high vacuum radio frequency oxygen plasma device. An oxygen plasma was applied for 30 minutes at a power of 50 W, using a chamber pressure of 1.2×10^{-2} mbar. The sample was simultaneously heated on the stage; 50 °C for the first 5 minutes, and then 300 °C for the remainder of the treatment (25 mins). These 1cm² flat silicon (111) substrates with patterned arrays of gold nanoparticles were then subsequently analysed using GIWAXS/GISAXS under *operando* conditions for butadiene hydrogenation.

Characterisation and Analysis

Grazing incidence small-angle X-ray scattering (GISAXS) and wide-angle X-ray scattering (GIWAXS). *Operando* GISAXS and GIWAXS experiments were conducted at the I07 beamline, Diamond Light Source, with a configuration similar to that previously

used by Arnold et al.[2] The photon energy was 10 keV. The focused beam of ca. 0.3×0.3 mm^2 was directed on the sample at an incident angle α of 0.15° and 0.30°. The sample to detector distance (SD) was calibrated using several diffraction orders of Ag behenate. The modulus of the scattering vector **q** was calculated as q = 4πsin θ/λ, where θ is the Bragg angle and λ - the wavelength of the photons. GISAXS was collected using a large area detector (Pilatus 2M, 172×172 μm^2 pixel size, 1673×1475 pixels) at a distance of 2685 mm. GIWAXS was collected using a small swing arm area detector (Pilatus 100K, 172×172 μm^2 pixel size, 487×195 pixels).

The samples were positioned inside a sealed reactor complete with X-ray transparent mica windows equipped with a computer controlled heating stage (Fig. S1). The reactor was connected to a purpose built gas delivery system comprising of switching valves and mass flow controllers which enabled complete control of gas mixing and flow rates. The exit of the reactor was coupled to a mass spectrometer (Pfeiffer, Quadstar 422). GIWAXS/GISAXS were recorded at different gas compositions and catalysis operating temperatures. The sample temperature was 473 K unless stated otherwise. The order was as follows; calcination in helium (He) 548K at flow rate 100 ml/min, hydrogen H$_2$ (5% in He) and He at flow rate ratio 50/4 ml/min, butadiene (5% in He) and He at flow rate ratio 4/50 ml/min, hydrogen and butadiene (catalysis) at flow rate ratio 50/4 ml/min, and then clean catalyst afterwards with He gas at 54 ml/min. Butenes were verified as catalytic products using online mass spectrometry, however quantitative analysis was not performed. The GISAXS/GIWAXS reactor was optimised for characterisation, and not for catalysis, and thus conversion to butenes was only moderate. At each step, five areas were scanned laterally in 0.25 mm increments and the signal was averaged, and then radially integrated using the 'DAWN Science' package.[3] Reduced 1D GIWAXS profiles were fitted using Voigt function in the OriginPro. Data were visualised in Igor Pro.

The GISAXS data were fitted using IsGISAXS software.[4] To analyse 2D GISAXS image two cuts at the constant q$_z$ (parallel cut) and q$_{x,y}$ (perpendicular cut) have been fitted simultaneously. Figure 1b shows structural model of the catalyst with the spherical AuNPs embedded into the Si support and forming hexagonal superlattice with the parameter of ca. 70 nm. The initial input parameters such as NPs radius, height and interparticle distance were taken from the microscopy data (Fig. 1 & S2).

For the highly monodispersed NPs we assume their size and shape vary slowly across the sample. In this case one can use the Local Monodisperse Approximation (LMA) to calculate the scattering cross-section σ: [5]

$$\frac{d\sigma}{d\Omega}(q) \cong \langle |F(q)^2| \rangle_\alpha S(q)$$
(1)

where Ω is solid angle around (θ, α), **q** - scattering vector, F(**q**) –form factor of the nanoparticle, S(**q**) – interference function.

To account for multiple reflection-refraction effects on the surface of the flat SiO$_2$/Si substrate one can use the Distorted Wave Born Approximation (DWBA) framework.[6] The effective form factor with the four terms associated with the different reflection scenarios of incident or scattered beam reads as follows:

$$F\left(q_{xy}, k_z^i, k_z^f\right) = F\left(q_{xy}, k_z^f - k_z^i\right) + r(\alpha_i)F\left(q_{xy}, k_z^f + k_z^i\right) + r(\alpha_f)F\left(q_{xy}, -k_z^f - k_z^i\right) + r(\alpha_i)r(\alpha_f)F\left(q_{xy}, -k_z^f + k_z^i\right)$$
(2)

where $\mathbf{q_{xy}}$ is in-plane component of the scattering vector $q_{xy} = \sqrt{q_x^2 + q_y^2}$; $\mathbf{k^i}$ and $\mathbf{k^f}$ are the incident and outgoing wavevectors respectively; r(α) – Fresnel reflection coefficient. The refractive indices of Si, SiO_2, Au were taken from the literature.[7]
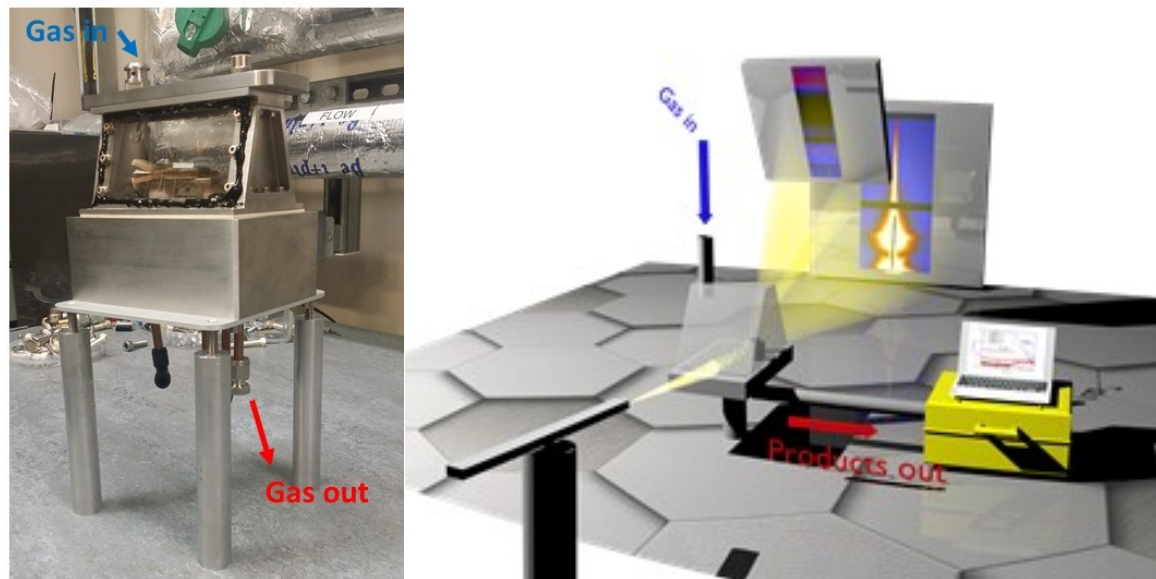
Figure S1: (Left) Photograph of the reactor cell at the I07 beamline (DLS) used in catalytic experiments. Gas enters from the top, and exits via the bottom. A pressure relief valve is located at the top to prevent pressure being put on the mica windows. The cell is sealed with an epoxy resin to maintain a specific atmosphere. (Right) Artist's impression of the *operando* grazing incidence X-ray scattering set up used in this study.

Scanning Electron Microscopy (FESEM) micrographs were recorded with a JEOL JSM-7401F field emission gun scanning electron microscope at acceleration voltage of 2.0 kV, using both secondary electron and backscattered electron detectors to achieve contrast between substrate and nanoparticle. Particle size analysis was conducted on ImageJ.[8]

Atomic Force Microscopy (AFM). Au NPs supported on Si(111) substrates were investigated under ambient conditions using a Bruker Veeco Dimension 3100 instrument in tapping mode. Data processing was conducted using the Nanoscope software.

X-ray photoelectron spectroscopy (XPS). Measurements were done on a Thermoscientific XPS K-alpha surface analysis photoelectron spectrometer under ultrahigh vacuum ($< 5 \times 10^8$ Torr) and by using a monochromatic Al K-Alpha X-ray source. XPS area mapping (6 points in total) was used, using a point-to-point distance of 0.7mm, in order to give an average, homogenized data set. Analysis was performed on the Thermo Advantage and CasaXPS software packages. Data was calibrated to an adventitious carbon 1s peak at to 284.4 eV and used as an internal standard to compensate for any charging effects.

Results

Surface and morphology of the Au/SiO$_2$-Si(111) model catalyst.
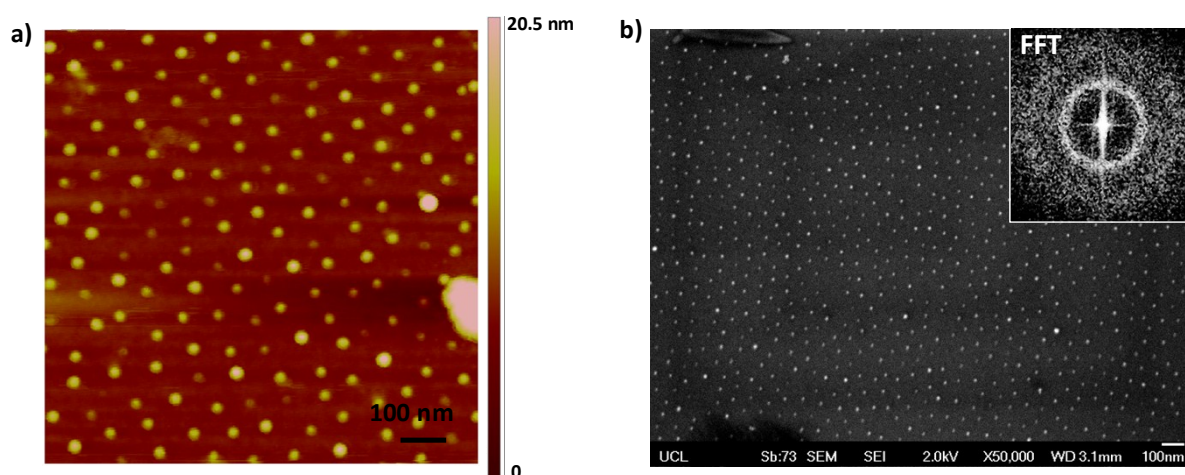
Figure S2: (a) AFM height image of the Au/SiO$_2$-Si(111) supports used in the catalytic studies. Average measured height H = 6.2 ± 0.5 nm (ca. 150 particles measured); (b) FESEM micrograph of AuNPs on SiO2-Si(111). Calculated particle size D = 9.0 ± 0.9 nm and interparticle distance 78.8 ± 9.9 nm. Inset: FFT of the SEM micrograph
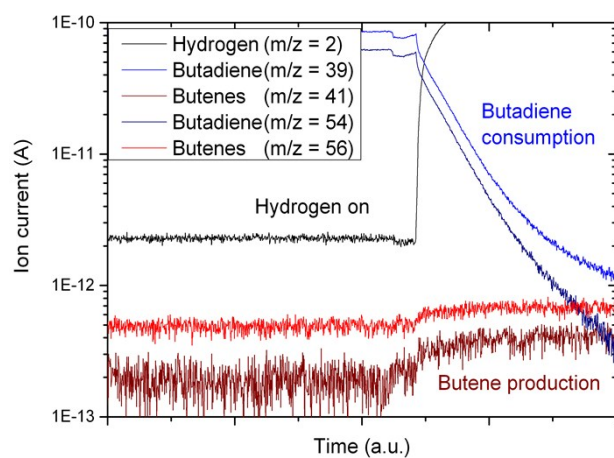
Figure S3. MS data shows the activity of Au/SiO$_2$-Si model catalyst during the hydrogenation of butadiene. Two signals are used for both butadiene and butenes.

GISAXS

Grazing-incidence small-angle (GISAXS) and wide-angle X-ray scattering (GIWAXS) are powerful techniques for probing interfaces and morphology of the nanometer thin films, but to the best of our knowledge, not been applied to study catalysts under *operando* conditions.[9–15] Several studies exist whereby GISAXS/GIWAXS have been used to investigate nanoparticle growth, and population analysis reveals local and global changes in the system[11,16,17]. The power of this combined technique lies in the sensitivity to both changes in particle shape and size, and also *inter-particle* separation due to coalescence, sintering and metal-support effects[18,19]. Perhaps the most striking example of GI techniques was demonstrated by Nolte et al whom showed that a combination of surface X-ray diffraction (SXRD) and GISAXS reveal *shape* changes in Rh nanoparticles under simple reducing and oxidizing atmospheres[10]. Interestingly, a particle *size* change was not observed in the GISAXS data, most likely due to the relatively mild reduction/oxidation conditions (e.g. *mbar* pressures of CO or O_2).

Table S1. Summary of the structural parameters for Au/SiO_2-Si(111) catalyst resulting from fitting the experimental 2D GISAXS data using DWBA formalism.

Gas	R, nm	σ_R (lognorm), nm	H/R	σ_H (Gauss), nm	L_{hex}, nm	ω_{2DDL}, nm
Helium (He)	4.22 ± 0.16	1.11 ± 0.06	1.14 ± 0.03	0.09 ± 0.02	74.20 ± 0.12	11.86 ± 0.12
Butadiene (C_4H_6)	4.22 ± 0.16	1.12 ± 0.05	1.14 ± 0.03	0.05 ± 0.03	74.20 ± 0.11	12.02 ± 0.12
$C_4H_6 + H_2$	4.67 ± 0.04	1.4 ± 0.01	2.0 ± 0.42	0.53 ± 0.04	74.20 ± 0.04	12.55 ± 0.04
post He (repeat)	3.98 ± 0.54	1.03 ± 0.07	1.24 ± 0.17	0.06 ± 0.01	73.59 ± 0.03	13.32 ± 0.03

R - radius of the AuNPs
H - height of the AuNPs above the SiO2 substrate
σ_R –width of lognormal distribution for R
σ_H - width of gaussian distribution for H
L_{hex} – parameter of the hexagonal superlattice formed by AuNPs
ω – interference function parameter for the 2D hexagonal lattice

Crystalline structure and composition of the supported Au/SiO_2-Si(111) catalyst

GIWAXS

Table S2. Areas of the (200) peak of gold FCC lattice and (111) peak of Au_2O_3 orthorhombic lattice for Au/SiO_2-Si catalyst under various gas atmospheres.

Gas	Area Au (200) peak, (a.u.)	Area Au_2O_3 (111) peak, (a.u.)
Helium (He)	293.7 ± 13.4	59.4 ± 3.9
Hydrogen (H_2)	222.3 ± 72.8	56.0 ± 4.1
Butadiene (C_4H_6)	235.6 ± 58.3	44.6 ± 3.5
$C_4H_6 + H_2$	301.2 ± 9.2	40.0 ± 3.5
post He (repeat)	224.9 ± 62.4	37.7 ± 3.3
He (room temperature)	207.8 ± 12.3	54.4 ± 3.9

XPS analysis

Ono and Cuenya used X-ray photoelectron spectroscopy (XPS) to show that Au_2O_3 can in fact be stable on oxygen plasma treated Au nanoparticles (*ca.* 5 nm) supported on SiO_2[20]. Both surface and subsurface gold oxide was thought to be present, with the former decomposing below 600 K, and the latter remaining within the 'bulk' even after heating. Therefore, it is not unlikely that here, there is actually a migration/partial removal of an Au_2O_3 layer during catalysis, which reemerges after the catalytic hydrogenation of butadiene. It was confirmed using the Au 4f photoelectron excitation that there exists two species of gold on Au/SiO_2-Si; metallic Au^0 (84.0 and 87.7 eV) and oxidic Au^{III} (85.6 and 88.8 eV) as shown in Fig. S5 and Table S4. Furthermore, the dominant oxygen species according to the O 1s spectra is ozone/O_3; typical of oxygen plasma treated supports[21]. As assumed, the area surrounding Au nanoparticles is mostly composed of a native SiO_2 layer[22,23].
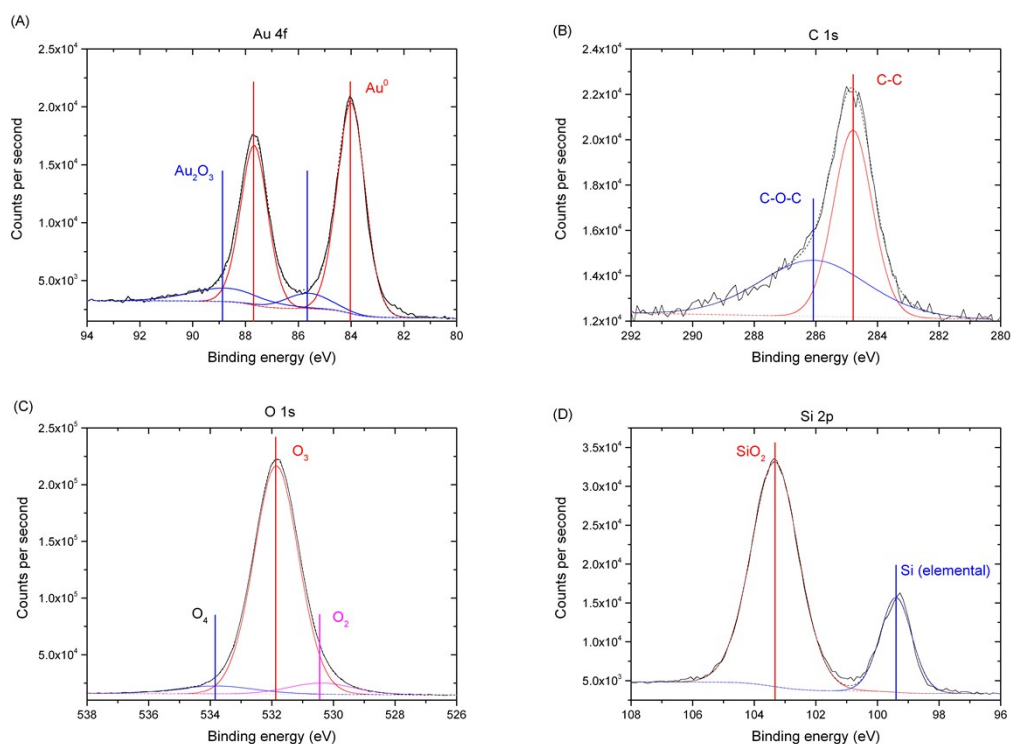
Figure S4. XPS spectra of (A) Au 4f, (B) C 1s, (C) O 1s and (D) Si 2p.

Table S3. Summary of XPS analysis for Au/SiO_2-Si catalyst. Atomic concentration is given as a percentage of the total integrated area in all instances.

	Peak	Position (eV)	%At conc.	%sum	Chemical state ([reference])
Gold	Au 4f	84.0	49.5	86.0	Metallic ([22])
	Au 4f	87.7	36.5		
	Au 4f	85.6	5.8	14.0	Oxidic ([24])
	Au 4f	88.8	8.3		

Carbon	C 1s	284.8	54.8		C-C ([25])
	C 1s	286.1	45.2		C-O([25])
Oxygen	O 1s	531.9	88.4		O_3 ([21])
	O 1s	533.8	5.3		O_4([21])
	O 1s	530.4	6.3		O_2([21])
Silicon	Si 2p	103.3	78.0		SiO_2 ([22,23])
	Si 2p	99.4	22.0		Elemental Si ([22,23])

References

1   J. P. Spatz, S. Mössmer, C. Hartmann, M. Möller, T. Herzog, M. Krieger, H. G. Boyen, P. Ziemann and B. Kabius, *Langmuir*, 2000, **16**, 407–415.

2   T. Arnold, C. Nicklin, J. Rawle, J. Sutter, T. Bates, B. Nutter, G. McIntyre and M. Burt, *J. Synchrotron Radiat.*, 2012, **19**, 408–416.

3   M. Basham, J. Filik, M. T. Wharmby, P. C. Y. Chang, B. El Kassaby, M. Gerring, J. Aishima, K. Levik, B. C. A. Pulford, I. Sikharulidze, D. Sneddon, M. Webber, S. S. Dhesi, F. Maccherozzi, O. Svensson, S. Brockhauser, G. Náray and A. W. Ashton, *J. Synchrotron Radiat.*, 2015, **22**, 853–858.

4   R. Lazzari, *J. Appl. Crystallogr.*, 2002, **35**, 406–421.

5   J. S. Pedersen, *J. Appl. Crystallogr.*, 1994, **27**, 595–608.

6   S. K. Sinha, E. B. Sirota, S. Garoff and H. B. Stanley, *Phys. Rev. B*, 1988, **38**, 2297–2311.

7   B. L. Henke, E. M. Gullikson and J. C. Davis, *At. Data Nucl. Data Tables*, 1993, **54**, 181–342.

8   M. D. Abràmoff, P. J. Magalhães and S. J. Ram, *Biophotonics Int.*, 2005, **11**, 36–43.

9   S. Mostafa, F. Behafarid, J. R. Croy, L. K. Ono, L. Li, J. C. Yang, A. I. Frenkel and B. R. Cuenya, *J. Am. Chem. Soc.*, 2010, **132**, 15714–15719.

10 P. Nolte, A. Stierle, N. Y. Jin-Phillipp, N. Kasper, T. U. Schulli, H. Dosch, T. The and T. Landau, *Sci.*, 2008, **321**, 1654–1658.

11 I. Laoufi, M. C. Saint-Lager, R. Lazzari, J. Jupille, O. Robach, S. Garaudée, G. Cabailh, P. Dolle, H. Cruguel and A. Bailly, *J. Phys. Chem. C*, 2011, **115**, 4673–4679.

12 R. Wojcieszak, M. J. Genet, P. Eloy, P. Ruiz and E. M. Gaigneaux, *J. Phys. Chem. C*, 2010, **114**, 16677–16684.

13 S. J. Tinnemans, J. G. Mesu, K. Kervinen, T. Visser, T. A. Nijhuis, A. M. Beale, D. E. Keller, A. M. J. Van Der Eerden and B. M. Weckhuysen, *Catal. Today*, 2006, **113**, 3–15.

14 S. Fall, L. Biniek, Y. Odarchenko, D. V. Anokhin, G. de Tournadre, P. Lévêque, N. Leclerc, D. A. Ivanov, O. Simonetti, L. Giraudet and T. Heiser, *J. Mater. Chem. C*, 2016, **4**, 286–294.

15 J. Wang, Y. I. Odarchenko, M. Defaux, J. Lejnieks, D. V. Ahokhin, H. Keul, D. A. Ivanov, M. Möller and A. Mourran, *Macromolecules*, 2013, **46**, 6159–6168.

16 G. Renaud, R. Lazzari, C. Revenant, A. Barbier, M. Noblet, O. Ulrich, F. Leroy, J. Jupille, Y. Borensztein, C. R. Henry, J.-P. Deville, F. Scheurer, J. Mane-Mane and O. Fruchart, *Science (80-.).*, 2003, **300**, 1416–9.

17 S. A. Wyrzgol, S. Schäfer, S. Lee, B. Lee, M. Di Vece, X. Li, S. Seifert, R. E. Winans, M. Stutzmann, J. A. Lercher and S. Vajda, *Phys. Chem. Chem. Phys.*, 2010, **12**, 5585–95.

18 L. M. Molina, S. Lee, K. Sell, G. Barcaro, A. Fortunelli, B. Lee, S. Seifert, R. E. Winans,

J. W. Elam, M. J. Pellin, I. Barke, V. von Oeynhausen, Y. Lei, R. J. Meyer, J. A. Alonso, A. Fraile Rodríguez, A. Kleibert, S. Giorgio, C. R. Henry, K.-H. Meiwes-Broer and S. Vajda, *Catal. Today*, 2011, **160**, 116–130.

19   R. E. Winans, S. Vajda, G. E. Ballentine, J. W. Elam, B. Lee, M. J. Pellin, S. Seifert, G. Y. Tikhonov and N. A. Tomczyk, *Top. Catal.*, 2006, **39**, 145–149.

20   L. K. Ono and B. R. Cuenya, *J. Phys. Chem. C*, 2008, **112**, 4676–4686.

21   G. Forte, A. Travaglia, A. Magrì, C. Satriano and D. La Mendola, *Phys. Chem. Chem. Phys.*, 2013, **16**, 1536–44.

22   A. R. Gonzalez-Elipe, J. P. Espinos, G. Munuera, J. Sanz and J. M. Serratosa, *J. Phys. Chem.*, 1988, **92**, 3471–3476.

23   C. D. Wagner, D. E. Passoja, H. F. Hillery, T. G. Kinisky, H. A. Six, W. T. Jansen and J. A. T. Auger, *Sci. Technol*, 1982, **21**, 933–944.

24   B. Roldan Cuenya and F. Behafarid, *Surf. Sci. Rep.*, 2015, **70**, 135–187.

25   C. J. Powell, *J. Electron Spectros. Relat. Phenomena*, 2012, **185**, 1–3.